1521-009X/45/3/260–268$25.00
Drug Metabolism and Disposition
http://dx.doi.org/10.1124/dmd.116.073890
Drug Metab Dispos 45:260–268, March 2017

Application of Static Modeling in the Prediction of In Vivo Drug–Drug Interactions between Rivaroxaban and Antiarrhythmic Agents Based on In Vitro Inhibition Studies

Eleanor Jing Yi Cheong, Janice Jia Ni Goh, Yanjun Hong, Gopalakrishnan Venkatesan, Yuanjie Liu, Gigi Ngar Chee Chiu, Pipin Kojodjojo, and Eric Chun Yong Chan

Department of Pharmacy, Faculty of Science, National University of Singapore, Singapore (E.J.Y.C., J.J.N.G., Y.H., G.V., Y.L., G.N.C.C., E.C.Y.C.); Department of Chemistry, Faculty of Science, Hong Kong Baptist University, Ho Sin Hang Campus, Hong Kong (Y.H.); Department of Cardiology and Cardiac Electrophysiology, National University Heart Centre, Singapore (P.K.); and Singapore Institute for Clinical Sciences, Brenner Centre for Molecular Medicine, Singapore (E.C.Y.C.)

Received October 12, 2016; accepted December 21, 2016

ABSTRACT

Rivaroxaban, a direct Factor Xa inhibitor, is indicated for stroke prevention in nonvalvular atrial fibrillation (AF). Studies have revealed that the clearance of rivaroxaban is largely attributed to CYP3A4, CYP2J2 metabolism, and P-glycoprotein (P-gp) efflux pathways. Amiodarone and dronedarone are antiarrhythmic agents employed in AF management. Amiodarone, dronedarone, and their major metabolites, *N*-desethylamiodarone (NDEA) and *N*-desbutyldronedarone (NDBD), demonstrate inhibitory effects on CYP3A4 and CYP2J2 with U.S. Food and Drug Administration–recommended probe substrates. In addition, both amiodarone and dronedarone are known P-gp inhibitors. Hence, the concomitant administration of these antiarrhythmic agents has the potential to augment the systemic exposure of rivaroxaban through simultaneous impairment of its clearance pathways. Currently, however, clinical data on the extent of these postulated drug–drug interactions are lacking. In this study, in vitro inhibition assays using rivaroxaban as the probe substrate demonstrated that both dronedarone and NDBD produced reversible inhibition as well as irreversible mechanism-based inactivation of CYP3A4- and CYP2J2-mediated metabolism of rivaroxaban. However, amiodarone and NDEA were observed to cause reversible inhibition as well as mechanism-based inactivation of CYP3A4 but not CYP2J2. In addition, amiodarone, NDEA, and dronedarone, but not NDBD, were determined to inhibit P-gp–mediated rivaroxaban transport. The in vitro inhibition parameters were fitted into a mechanistic static model, which predicted a 37% and 31% increase in rivaroxaban exposure due to the inhibition of hepatic and gut metabolism by amiodarone and dronedarone, respectively. A separate model quantifying the inhibition of P-gp–mediated efflux by amiodarone or dronedarone projected a 9% increase in rivaroxaban exposure.

Introduction

Atrial fibrillation (AF) is the most commonly sustained and clinically significant cardiac arrhythmia, affecting approximately 33.5 million people worldwide in 2010 (Chugh et al., 2014). As the prevalence of AF increases with age, the global burden of the disease is projected to increase exponentially, creating a significant public health burden (Rahman et al., 2014). Therapeutic cornerstones of AF management include ventricular rate control, maintenance of sinus rhythm using antiarrhythmic therapy, and prevention of stroke and systemic embolism using anticoagulants (January et al., 2014).

Rivaroxaban (Xarelto; Janssen Pharmaceuticals, Inc., Beerse, Belgium), an inhibitor of Factor Xa of the coagulation cascade, was approved by the U.S. Food and Drug Administration (FDA) in 2011 as a novel non–vitamin K oral anticoagulant. Rivaroxaban is indicated for the reduction of risk of stroke and systemic embolism in patients with nonvalvular AF (FDA, 2011b). Studies have revealed that approximately two-thirds of the administered rivaroxaban dose undergoes metabolic clearance in the liver, with contributions from cytochrome P450 (P450) enzymes—namely, CYP3A4, CYP2J2, and hydrolytic enzymes (Weinz et al., 2009). The remaining one-third of the given dose is eliminated in the urine largely via P-glycoprotein (P-gp) and breast cancer resistance protein (ABCG2)–mediated secretion (Gnoth et al., 2011). A previous physiologically based pharmacokinetic (PBPK) modeling study characterized a drug–drug–disease interaction, in which the synergistic combination of renal impairment coupled with moderate CYP3A4 inhibition culminated in a clinically significant increase in rivaroxaban exposure (Grillo et al., 2012). Outcomes of this simulation eventually led to recommendations cautioning against the concomitant administration of moderate CYP3A4/P-gp inhibitors with rivaroxaban in

This research was supported by the Singapore Ministry of Education [Tier 1 Academic Research Funding, Grant R-148-000-193-112] and the National University of Singapore Department of Pharmacy [Final Year Project Funding, Grant C-148-000-003-001 (to E.C.Y.C.)].

E.J.Y.C., J.J.N.G., and Y.H. contributed equally to this work.

dx.doi.org/10.1124/dmd.116.073890.

This article has supplemental material available at dmd.aspetjournals.org.

ABBREVIATIONS: ACN, acetonitrile; AF, atrial fibrillation; AUC, area under the curve; AUCR, area under the curve ratio; DDI, drug–drug interaction; DMEM, Dulbecco's modified Eagle's medium; LC, liquid chromatography; MBI, mechanism-based inactivation; MDCK, Madin-Darby canine kidney; MDR, multidrug resistance protein; MS/MS, tandem mass spectrometry; NDBD, *N*-desbutyldronedarone; NDEA, *N*-desethylamiodarone; P-gp, P-glycoprotein; P450, cytochrome P450; P_{app}, apparent permeability; PBPK, physiologically based pharmacokinetic; rP450, recombinant cytochrome P450.

the presence of any degree of renal impairment (FDA, 2011b). This attests to the inherent susceptibility of rivaroxaban to complex drug–drug interactions (DDIs) mediated through simultaneous impairment of its multiple clearance pathways. Given the steep relationship between rivaroxaban exposure and major bleeding (FDA, 2011a), it is thus imperative to identify clinically relevant DDI scenarios that could augment rivaroxaban exposure.

A subgroup analysis of the ROCKET AF trial (Rivaroxaban Once Daily Oral Direct Factor Xa Inhibition Compared with Vitamin K Antagonism for Prevention of Stroke and Embolism Trial in Atrial Fibrillation) studying the efficacy and safety of rivaroxaban highlighted the potential combination of antiarrhythmic drug therapy and anticoagulation as mainstays in AF management and concluded that the concomitant use of amiodarone and rivaroxaban warrants further investigation (Steinberg et al., 2014). Dronedarone (Multaq; Sanofi Aventis, Bridgewater, NJ) was approved in 2009 as a structural analog of amiodarone (FDA, 2009a). In a bid to minimize the extracardiac adverse effects associated with amiodarone, iodine substituents were eliminated to avoid amiodarone-linked thyroid toxicities and a methanesulfonamide group was added to reduce tissue accumulation (Fig. 1, A and B) (FDA, 2009a).

Both amiodarone (Fig. 1A) and dronedarone (Fig. 1B) undergo extensive metabolism by CYP3A4/3A5 to form pharmacologically active metabolites *N*-desethylamiodarone (NDEA) (Fig. 1C) and *N*-desbutyldronedarone (NDBD) (Fig. 1D), respectively (Fabre et al., 1993; Klieber et al., 2014). In addition, both drugs are substrates of CYP2J2 (Lee et al., 2010; Karkhanis et al., 2016). The common structural features in these antiarrhythmic agents and their metabolites are the alkylamine and furan that are in turn associated with mechanism-based inactivation (MBI) of P450 (Orr et al., 2012). Indeed, corroborating previous findings, our laboratory established the reversible and irreversible inhibition of CYP3A4- and CYP2J2-mediated metabolism of FDA-recommended probe substrates by amiodarone and NDEA (Ohyama et al., 2000; McDonald et al., 2015; Karkhanis et al., 2016) as well as dronedarone and NDBD (Hong et al., 2016; Karkhanis et al., 2016). Independently, amiodarone and dronedarone have been reported as P-gp inhibitors (FDA, 2009b, 2012).

Taken together, we hypothesized that amiodarone, dronedarone, NDEA, and NDBD could increase systemic exposure of rivaroxaban via their inhibitory effects on CYP3A4, CYP2J2, and P-gp. To date, there remains a paucity of clinical data on the DDIs between rivaroxaban and these antiarrhythmic agents. This study aimed to quantitatively predict the in vivo DDI risk between rivaroxaban and amiodarone or dronedarone via mechanistic static modeling. To characterize the multifaceted DDIs and generate the inhibitory parameters accurately, rivaroxaban was used as the probe substrate in place of the respective FDA-recommended probe substrates of CYP3A4, CYP2J2, and P-gp.

Materials and Methods

In this study, in vitro inhibition data encompassing reversible inhibition, MBI, and inhibition of P-gp–mediated efflux were fitted into mechanistic static models that provided the framework for quantitative predictions of either metabolic or transporter-based DDIs between rivaroxaban and the antiarrhythmic drugs.

Chemicals. High-performance liquid chromatography (LC)–grade acetonitrile (ACN) was purchased from Tedia Company Inc. (Fairfield, OH). Amiodarone hydrochloride, dronedarone hydrochloride, NDBD, NDEA, rivaroxaban, and verapamil hydrochloride were acquired from Sigma-Aldrich (St. Louis, MO). Amprenavir was purchased from Toronto Research Chemicals Inc. (Toronto, ON, Canada). Human recombinant cytochrome P450 (rP450) supersomes and an NADPH regenerating system consisting of NADPH A ($NADP^+$ and glucose-6-phosphate) and B (glucose-6-phosphate dehydrogenase) were obtained from BD Gentest (Woburn, MA). Water was obtained using a Milli-Q water purification system (Millipore, Billerica, MA). For cell culture, Dulbecco's modified Eagle's medium (DMEM) with phenol red, Dulbecco's phosphate buffer solution, fetal bovine serum, and 10,000 IU antibiotic solution (penicillin/streptomycin) were obtained from Gibco Life Technologies (Waltham, MA). Lucifer yellow CH dilithium salt was from Invitrogen Corporation (Carlsbad, CA). L-Glutamine was from HyClone Laboratories (Logan, UT). Sodium bicarbonate powder was from Sigma-Aldrich (St. Louis, MO). All other reagents were of analytical grade.

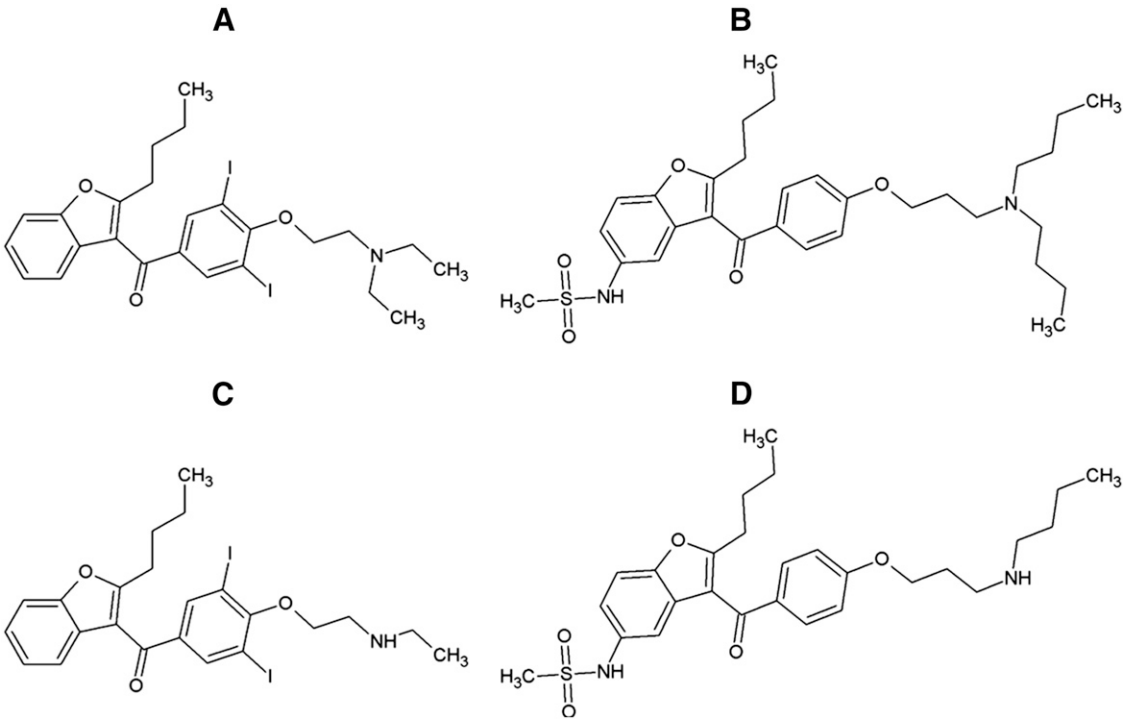

Fig. 1. Chemical structures of (A) amiodarone, (B) dronedarone, (C) NDEA, and (D) NDBD.

Reversible Inhibition of CYP3A4 and CYP2J2 by Amiodarone, Dronedarone, and Their Metabolites. Amiodarone, dronedarone, and their metabolites (i.e., NDEA and NDBD) were tested as reversible inhibitors using rivaroxaban as the probe substrate. Experiments were performed in 96-well plates and all samples were carried out in triplicates. Rivaroxaban (2.5, 5, 15, 30, and 50 μM) was preincubated at 37°C for 5 minutes with 20 pmol/ml rP450 enzymes, NADPH B, and 100 mM potassium phosphate buffer (pH 7.4) across multiple concentration levels of the inhibitors (amiodarone: 0–5 μM; dronedarone, NDEA, and NDBD: 0–10 μM). The reactions were initiated by the addition of 5 μl NADPH A, yielding a final incubation mixture of 100 μl with 1% ACN (v/v). Incubation was carried out at 37°C for either 2 hours with CYP3A4 or 30 minutes with CYP2J2 before an 80-μl aliquot was removed and quenched with an equal volume of ice-cold ACN containing 0.005 μM verapamil (internal standard). The quenched samples were subjected to centrifugation at 2755*g* at 4°C for 30 minutes. Subsequently, the supernatants were removed to determine the morpholinone hydroxylated metabolite (main metabolite) of rivaroxaban by LC–tandem mass spectrometry (MS/MS) analysis (Supplemental Methods; Supplemental Table 1). The data were first fitted to the Michaelis–Menten model. Subsequently, Lineweaver–Burk plots were applied to predict the mode of reversible inhibition. The apparent equilibrium dissociation constant (K_i) for the enzyme-inhibitor complex was determined by nonlinear least-squares regression based on the best model of reversible inhibition.

Time- and Concentration-Dependent Inactivation of CYP3A4 and CYP2J2 by Amiodarone, Dronedarone, and Their Metabolites. Rivaroxaban was used as the probe substrate in this experiment. Incubations (n = 3) were conducted in 96-well plates. Primary incubation mixtures comprising various concentration levels of amiodarone (0–5 μM) or NDEA (0–1 μM) were preincubated at 37°C for 5 minutes with rP450 enzymes (20 pmol/ml) and NADPH B in potassium phosphate buffer (100 mM, pH 7.4). To initiate the enzymatic reaction, 5 μl NADPH A was added to the primary incubation. The final primary incubation mixture volume was 100 μl and contained $<$ 1% (v/v) organic solvent. At different preincubation time points (0, 3, 8, 15, 22, 30, and 45 minutes) after the addition of NADPH A, 5-μl aliquots of the primary incubation were transferred to 95 μl of the secondary incubation containing 50 μM rivaroxaban, the NADPH regenerating system, and 100 mM potassium phosphate buffer (pH 7.4) to yield a 20-fold dilution. The secondary incubation mixtures were incubated at 37°C for 2 hours with CYP3A4 or 30 minutes with CYP2J2 before 80-μl aliquots were removed and quenched with an equal volume of ice-cold ACN containing 0.005 μM verapamil (internal standard). The same morpholinone hydroxylated metabolite was quantified using LC–MS/MS (Supplemental Methods; Supplemental Table 1). Inactivation of CYP3A4 (40 pmol/ml) and CYP2J2 (20 pmol/ml) by dronedarone (0–2.5 μM) and NDBD (0–5 μM) was investigated using the same two-step incubation protocol except with a 10-fold dilution into the secondary incubation.

Calculation of Inactivation Kinetic Parameters (K_I and k_{inact}). The mean of triplicate peak area ratios was normalized to 0 minutes with respect to preincubation time. The percentage of probe substrate activity remaining was computed and the natural logarithmic activity was plotted against inactivation preincubation time for each inactivator concentration. The data were fitted to a linear regression model, and k_{obs} values (apparent inactivation rate constants) were calculated as the negative slopes of the lines. Subsequently, a plot of k_{obs} values against inactivator concentration ([I]) allowed the fitting of inactivation kinetic parameters (K_I and k_{inact}) to nonlinear least-squares regression based on eq. 1 in GraphPad PRISM software (version 6.01; GraphPad Inc., San Diego, CA).

$$k_{obs} = \frac{k_{inact} \times [I]}{K_I + [I]} \quad (1)$$

In eq. 1, k_{inact} represents the maximum inactivation rate constant at infinite inactivator concentration, K_I is the concentration of inactivator at the half-maximum rate of inactivation, and [I] is the in vitro inactivator concentration.

Inhibition of P-gp Efflux of Rivaroxaban by Amiodarone, Dronedarone, and Their Metabolites. Madin-Darby canine kidney (MDCK) subclone I cells transfected with multidrug resistance protein (MDR) 1 were maintained in DMEM culture media supplemented with 10% fetal bovine serum, L-glutamine (862 mg/l), and 1% penicillin/streptomycin. For transport studies, cells were first seeded at a density of 250,000 cells/well and the culture medium was refreshed after 24 hours. At approximately 48 hours postseeding, the culture medium was first removed and each well and insert were rinsed gently with phosphate-buffered saline to ensure no residual metabolic waste. Test inhibitors were dissolved in methanol, whereas rivaroxaban was reconstituted in ACN and dimethylsulfoxide at lower (2 mM) and higher concentration (20 mM) levels, respectively. Dilutions for all compounds were carried out using ACN. Triplicate sets of wells were used to assess the apparent permeability (P_{app}) of rivaroxaban from the apical (A) to basolateral (B) chambers [P_{app} (A→B)] and B to A [P_{app} (B→A)]. To initiate transport, the donor solution was added first, followed by the receiver solution. All experiments were carried out at room temperature (24 ± 1°C). Amprenavir (10 μM) and propranolol (25 μM) were used as positive controls (substrate and inhibitor, respectively). P_{app} (A→B) of lucifer yellow (100 μM) was used as a marker of monolayer integrity. The fluorescence of lucifer yellow of each apical and basolateral solution was measured at an excitation wavelength of 430 nm and an emission wavelength of 540 nm using a Tecan Infinite F500 plate reader (Männedorf, Switzerland). Acceptance criterion for a confluent monolayer was defined as lucifer yellow permeability of $<$80 nm/s.

To ensure P-gp assay sensitivity, experiments were first performed to investigate the potential for both concentration- and time-dependent saturation of the transport of rivaroxaban via P-gp (Supplemental Methods). The optimal incubation time was eventually determined to be 90 minutes and a rivaroxaban concentration of 10 μM was also selected (Supplemental Figs. 1 and 2). Subsequently, 25 and 12.5 μM of each inhibitor (i.e., amiodarone, dronedarone, NDEA, and NDBD) was first subjected to a preliminary study to estimate the IC_{50} values. The inhibitor concentrations were subsequently optimized to encompass the IC_{50} and ensure inhibition assay sensitivity. The receiver solution was collected and stored at −20°C for further sample processing prior to LC–MS/MS analysis (Supplemental Methods). To determine the mode of P-gp inhibition, three inhibitor concentration levels in proximity of the IC_{50} value were assayed against two concentration levels of rivaroxaban (5 and 20 μM). A Dixon plot was generated to predict the mode of P-gp inhibition and to determine the K_i values.

Estimating the Extent of Metabolic DDIs Using a Mechanistic Static Model. The kinetic constants accounting for reversible inhibition (i.e., K_i) and time-dependent inactivation (i.e., k_{inact}, K_I) of the drug-metabolizing enzymes were incorporated into a mechanistic static model developed previously by Fahmi et al. (2008) and refined by Isoherranen et al. (2012) to account for multi-P450 inhibition. The proposed model accounts for the contributions of enzyme inhibition both in the liver and within the gut wall in predicting the extent of DDIs. The area under the curve ratio (AUCR) in the presence of a pharmacokinetic DDI is described by eq. 2:

$$\mathrm{AUCR} = \frac{1}{\sum_i^n \left[f_{m,P450i} \times (A \times B)\right] + \left(1 - \sum_i^n f_{m,P450i}\right)} \times \frac{1}{[X \times Y] \times (1 - F_G) + F_G} \quad (2)$$

The terms are defined as follows. A is the term for time-dependent inactivation observed in the liver for each of the P450 enzymes inactivated:

$$A = \frac{k_{deg,H}}{k_{deg,H} + \frac{[I]_H \times k_{inact}}{[I]_H + K_I}}$$

B is the term for reversible inhibition in the liver for each of the P450 enzymes inactivated:

$$B = \frac{1}{1 + \left([I]_H \div K_i\right)}$$

X is the term for time-dependent inactivation of CYP3A4 observed in the intestine:

$$X = \frac{k_{deg,G}}{k_{deg,G} + \frac{[I]_G \times k_{inact}}{[I]_G + K_I}}$$

Y is the term for reversible inhibition of CYP3A4 in the intestine:

$$Y = \frac{1}{1 + \left([I]_G \div K_i\right)}$$

where $[I]_H$ and $[I]_G$ represent in vivo concentrations of the inhibitor available to the enzyme in the liver and intestine, respectively (Table 1; Supplemental Table 2). The degradation rates for CYP3A4 in the liver ($k_{deg,H}$) and intestine ($k_{deg,G}$) were 0.00032 and 0.00048 min^{-1} based on a half-life of 36 hours and 24 hours, respectively (Fahmi et al., 2008). For CYP2J2, there are insufficient clinical pharmacokinetic data to perform similar calculations. As a result, the average of the calculated estimates for the various hepatic P450 enzymes (0.00026 min^{-1}) was used (Yang et al., 2008). The fraction of rivaroxaban metabolized by CYP3A4 ($f_{m,CYP3A4}$) and CYP2J2 ($f_{m,CYP2J2}$) was reported to be 0.18 and 0.14, respectively (Mueck et al., 2014), whereas the fraction of rivaroxaban escaping intestinal extraction (F_G) was calculated to be 0.89 (see the Supplemental Methods).

Estimating the Extent of Transporter-Mediated DDIs Using a Mechanistic Static Model. The kinetic constant describing the inhibition of P-gp–mediated efflux of rivaroxaban was fitted into another mechanistic static model developed to examine the effect of inhibition of renal secretion transporters on plasma exposure of the victim drug (Feng et al., 2013). The AUCR of the victim drug in the presence and absence of the inhibitor is summarized in eq. 3:

$$AUCR = \frac{1+\left(CL_{sec,c} \div CL_x\right)}{1+\frac{CL_{sec,c}}{CL_x} * \frac{1}{1+([I] \div K_i)}} = \frac{1}{1-\frac{CL_{sec,c}}{CL} * \frac{([I] \div K_i)}{1+([I] \div K_i)}} \quad (3)$$

where $[I]$ represents the maximum plasma concentration of the inhibitor (Table 1). The net secretory clearance of rivaroxaban ($CL_{sec,c}$) (55.6 ml/min) was approximated to be five-sixths of the total plasma renal clearance (66.7 ml/min) (Mueck et al., 2014). The total plasma clearance (CL) of rivaroxaban was reported to be 166.7 ml/min and is a composite of the hepatic and renal clearances (Mueck et al., 2014).

Results

Reversible Inhibition of CYP3A4 and CYP2J2 by Amiodarone, Dronedarone, and Their Metabolites. The reversible inhibition of CYP3A4 and CYP2J2 by amiodarone, dronedarone, and their metabolites was investigated using the peak area of rivaroxaban metabolite as a proxy for the rate of product formation. Rivaroxaban was evaluated across five concentration levels spanning its K_m in the presence of varying concentrations of amiodarone, dronedarone, NDEA, and NDBD. In a preliminary study of reversible inhibition of CYP2J2 by amiodarone and NDEA, high concentrations of both amiodarone and NDEA were easily overcome by a small increase in rivaroxaban concentration, thus suggesting that amiodarone and NDEA did not inhibit CYP2J2 with rivaroxaban as the probe substrate (Supplemental Fig. 3A). However, based on the inhibition kinetics plots (Fig. 2, A and B) and their respective Lineweaver–Burk plots (Fig. 2, C and D), dronedarone and NDBD were established to be mixed competitive inhibitors of CYP2J2 when rivaroxaban was used as the probe substrate. On the other hand, amiodarone and NDEA exhibited mixed competitive inhibition of CYP3A4 (Fig. 3, A, B, E, and F), whereas dronedarone and NDBD demonstrated competitive inhibition (Fig. 3, C, D, G, and H). The calculated inhibition constants K_i of the relevant inhibitors against the respective enzymes are presented in Table 2.

TABLE 1

Relevant in vivo concentrations of amiodarone, dronedarone, and their metabolites that were incorporated into mechanistic static models

Parameter	Amiodarone	NDEA	Dronedarone	NDBD
		μM		
$[I]_{H\ (inactivation)}$[a]	0.12	0.18	0.00063	0.0045
$[I]_{H\ (reversible\ inhibition)}$[b]	0.15	0.18[e]	0.021	0.0045[e]
$[I]_G$[c]	7.50	NA	40.4	NA
$[I]$[d]	2.99	2.80	0.21	0.21

Drug-dependent parameters necessary for the derivations of these in vivo concentrations are presented in Supplemental Table 2. NA, not applicable.

[a] $[I]_{H\ (inactivation)}$ is the concentration of inactivator at the enzyme active site in the liver defined as the systemic steady-state unbound peak plasma concentration ($f_{u,b} \times C_{ss,max}$).

[b] $[I]_{H\ (reversible\ inhibition)}$ is the concentration of inhibitor at the enzyme active site in the liver defined as the hepatic portal inlet steady-state unbound C_{max} [$f_{u,b} \times (D \times k_a \times F_a/Q_H) + C_{ss,max}$], where D is total daily oral dose of the inhibitor, k_a is the oral absorption rate constant, F_a is the product of the fractions absorbed and escaping intestinal metabolism, and Q_H is the hepatic blood flow (1450 ml/min).

[c] $[I]_G$ is the concentration of inactivator/inhibitor at the enterocyte during absorption defined as $D \times k_a \times f_a/Q_H$, where f_a is the fraction of the inactivator/inhibitor dose absorbed into the gut wall and Q_g is the enterocytic blood flow (248 ml/min).

[d] $[I]$ is the peak plasma concentration of the inhibitor.

[e] $[I]_{H\ (reversible\ inhibition)}$ for NDEA and NDBD is defined as the systemic steady-state unbound peak plasma concentration.

Time- and Concentration-Dependent Inactivation of CYP3A4 and CYP2J2 by Amiodarone, Dronedarone, and Their Metabolites. To investigate the MBI of CYP3A4 and CYP2J2 by amiodarone, dronedarone, and their metabolites, rivaroxaban was used as the probe substrate and the rate of hydroxylation at the morpholinone moiety of rivaroxaban was monitored and used as a surrogate for enzymatic activity. In the presence of NADPH, a time-dependent decrease in CYP2J2 enzymatic activity was not observed when preincubated with amiodarone (5 μM and 50 μM) and NDEA (Supplemental Fig. 3, B and C). However, time-dependent inactivation of CYP2J2 was demonstrated in the presence of dronedarone and NDBD. Preincubation of CYP2J2 with increasing concentration levels of either dronedarone or NDBD resulted in a concentration-dependent increased rate of inactivation of enzymatic activity. The observed first-order rates of inactivation (k_{obs}) calculated from various concentrations of dronedarone (Fig. 4A) and NDBD (Fig. 4B) followed saturation kinetics that approached a maximum rate of inactivation (Fig. 4, C and D). Likewise, as presented in Fig. 5, A–D, time- and concentration-dependent inactivation of CYP3A4 was established for both amiodarone, dronedarone, and their metabolites. Kinetic plots (k_{obs} versus inactivator concentration) also demonstrated saturation kinetics (Fig. 5, E–H). Calculated inactivation kinetic parameters, K_I and k_{inact}, are summarized in Table 3. The efficiency of enzyme inactivation (k_{inact}/K_I ratio) is also reported.

Cell Monolayer Integrity and Compound Recovery. A-to-B flux determinations of lucifer yellow were used to confirm monolayer integrity when coincubated with the highest concentration levels of the test substrate and inhibitors. These data confirmed that the monolayer was intact under these extreme conditions and validated its suitability for subsequent permeability studies. Using liquid-liquid extraction, a high recovery of rivaroxaban (approximately 100%) and accurate linear calibration ($\pm$20% accuracy and $r^2 = 0.99$) were achieved reproducibly from 0.01 to 10 μM. For rivaroxaban concentrations above 10 μM, saturation of the detector was observed and the samples were diluted using DMEM before sample processing to ensure its accurate quantitation. Percentage recovery of rivaroxaban from the apical and basolateral chambers at the end of the assay (mass balance) was $> 80\%$, indicating that no significant amount of rivaroxaban was lost during sample transfer and processing nor in MDCK-MDR1, hence demonstrating the reliability of measured P_{app} values.

P-gp Inhibitory IC_{50} and K_i of Test Inhibitors. The concentration-dependent inhibitory effect of amiodarone, dronedarone, and their metabolites on transport of rivaroxaban across MDR1-MDCKII monolayers was tested. IC_{50} is the inhibitor concentration needed to decrease the efflux ratio by half. Amiodarone (Fig. 6A) and NDEA (Fig. 6B) yielded similar IC_{50} values of 10.3 μM and 9.20 μM, respectively. Based on an IC_{50} of 1.83 μM (Fig. 6C), dronedarone was determined to be the most potent P-gp inhibitor, whereas NDBD demonstrated little P-gp inhibition activity, as seen from its high IC_{50} value of 76.3 μM (Fig. 6D). Subsequently, the respective inhibitory concentrations that produced a linear decrease in efflux ratio were chosen for the Dixon plots (data not shown), in which we confirmed amiodarone's noncompetitive allosteric inhibition of P-gp efflux of rivaroxaban (5 and 20 μM) with a

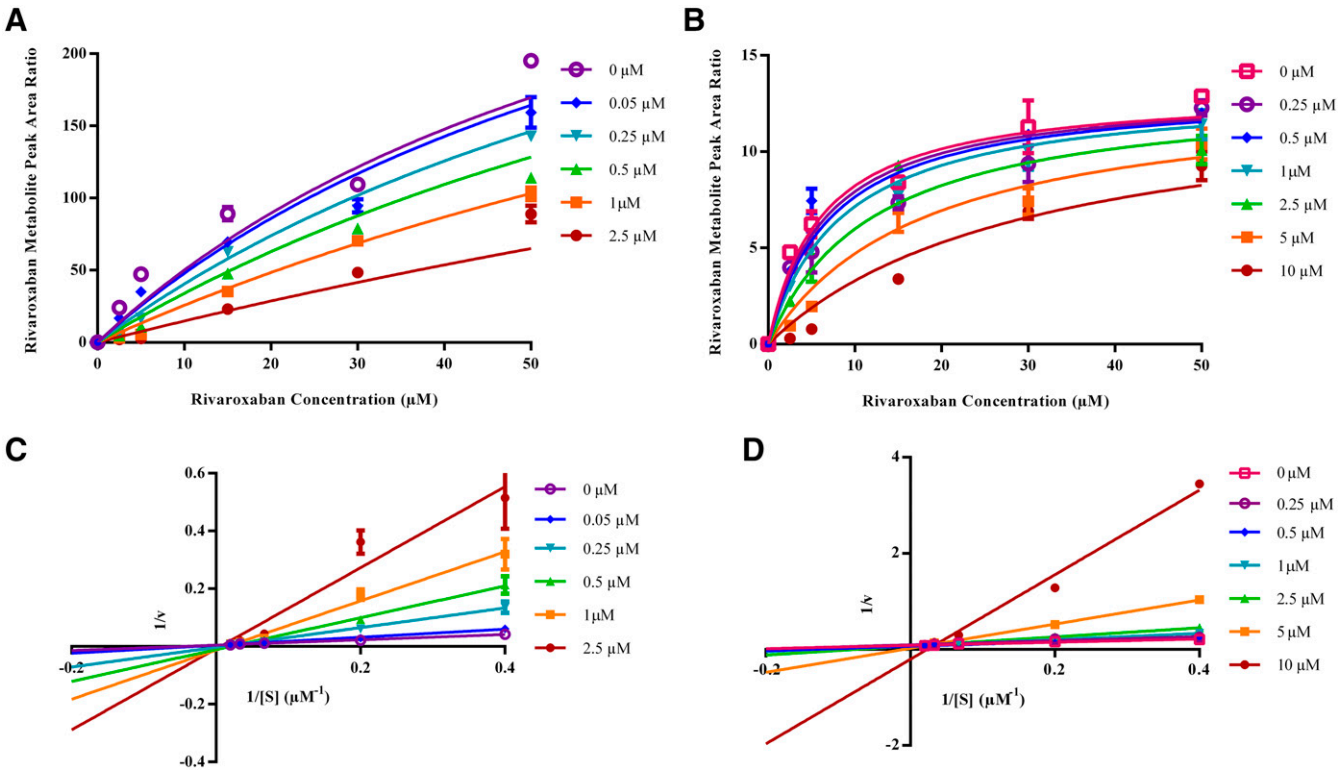

Fig. 2. Reversible inhibition of recombinant CYP2J2 (rCYP2J2) by dronedarone and NDBD. (A and B) The formation rate of the morpholinone hydroxylated metabolite was plotted against inhibitor concentration and fitted in the Michaelis–Menten kinetic model to calculate the inhibition constant K_i for (A) dronedarone and (B) NDBD toward rCYP2J2. (C and D) Lineweaver–Burk plots exhibit mixed competitive inhibition of rCYP2J2 by dronedarone and NDBD. Each point represents the mean ± S.D of triplicate experiments.

K_i at 8.94 μM, whereas dronedarone demonstrated competitive inhibition with a K_i at 0.68 μM. Assuming the same mode of noncompetitive inhibition of P-gp, the K_i value of NDEA was determined to be 5.36 μM. The K_i value of NDBD was not further elucidated, as its high IC_{50} value was predicted not to produce meaningful inhibitory potential.

Static Modeling of Metabolic and Transport-Based DDIs. In vitro inactivation (k_{inact} and K_I) and inhibition (K_i) parameters were subsequently incorporated into a mechanistic static model (eq. 2) that permits comprehensive evaluation of the potential impact of MBI and reversible inhibition of CYP3A4 and CYP2J2 on the systemic exposure of rivaroxaban. In the assessment of metabolic DDI potential using area under the curve (AUC) fold change, inhibition of hepatic metabolism of rivaroxaban by amiodarone, NDEA, dronedarone, and NDBD was predicted to produce AUC fold changes of 1.22, 1.22, 1.17, and 1.26 respectively (Table 4). When the combined effects of altered hepatic and intestinal metabolism were considered, there was an increase in the AUC fold change precipitated by amiodarone and dronedarone to 1.37 and 1.31, respectively (Table 4). Transporter-mediated DDI was quantitatively determined by fitting in vitro parameters describing inhibition of P-gp–mediated efflux of rivaroxaban into eq. 3. As summarized in Table 4, the eventual AUC fold change was 1.09 for both dronedarone and amiodarone, whereas NDEA produced a slightly higher AUC fold change of 1.13.

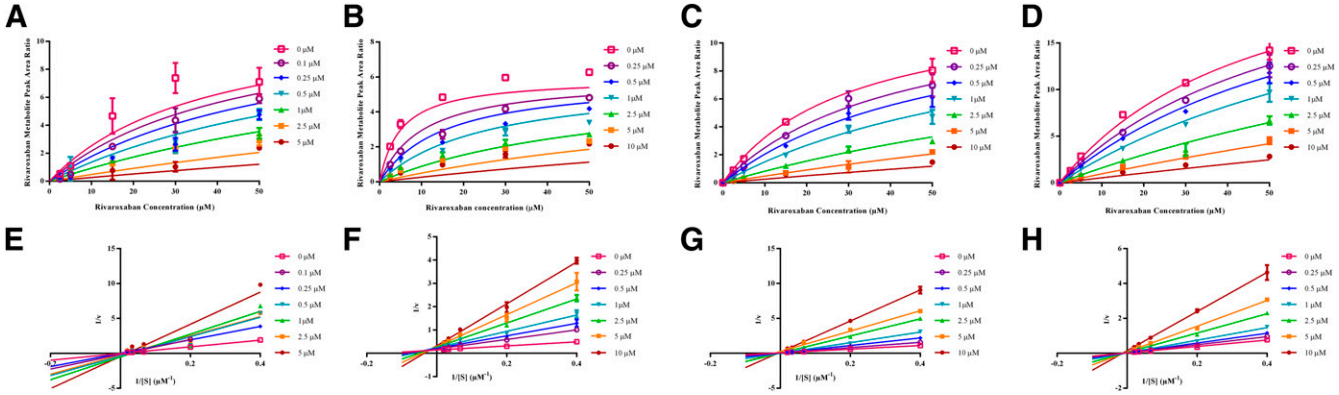

Fig. 3. Reversible inhibition of recombinant CYP3A4 (rCYP3A4) by amiodarone, NDEA, dronedarone, and NDBD. (A–D) The formation rate of the morpholinone hydroxylated metabolite was plotted against inhibitor concentration and fitted in the Michaelis–Menten kinetic model to calculate the inhibition constant K_i for (A) amiodarone, (B) NDEA, (C) dronedarone, and (D) NDBD toward rCYP3A4. (E–H) Lineweaver–Burk plots exhibit mixed competitive inhibition of rCYP3A4 by (E) amiodarone and (F) NDEA and competitive inhibition of rCYP3A4 by (G) dronedarone and (H) NDBD. Each point represents the mean ± S.D of triplicate experiments.

TABLE 2

CYP3A4 and CYP2J2 reversible inhibition kinetic parameters for amiodarone, NDEA, dronedarone, and NDBD using rivaroxaban metabolite peak area ratio as a surrogate measurement of product formation

Data represent means ± S.D.

P450	K_i
	μM
CYP3A4	
Amiodarone	0.226 ± 0.050
NDEA	0.239 ± 0.053
Dronedarone	0.64 ± 0.045
NDBD	1.03 ± 0.053
CYP2J2	
Amiodarone	NA
NDEA	NA
Dronedarone	0.93 ± 0.11
NDBD	2.53 ± 0.33

NA, not applicable.

Discussion

The application of in vitro methodologies to evaluate the inhibitory potential of a drug entity and assess the likelihood of in vivo drug interactions is a critical aspect of the drug development and regulatory review paradigm (Zhang et al., 2009). In this study, we quantified the in vitro inhibition parameters to characterize the DDI between rivaroxaban and the antiarrhythmic agents.

Rivaroxaban was not tested as a substrate in previous in-house studies investigating the CYP3A4 and CYP2J2 inhibitory potencies of amiodarone, dronedarone, and their metabolites (Hong et al., 2016; Karkhanis et al., 2016). In this study, we observed a significantly slower rate of rivaroxaban clearance by CYP3A4 as compared with CYP2J2 during initial assay optimization (data not published). Our optimization culminated in two incubation time periods of 2 hours and 30 minutes for the sensitive detection of inhibitory effects against CYP3A4 and CYP2J2, respectively.

We report for the first time the competitive inhibition as well as MBI of CYP3A4 and CYP2J2 by dronedarone and NDBD with rivaroxaban as the probe substrate. On the other hand, amiodarone and NDEA demonstrated mixed competitive inhibition of CYP3A4 but not CYP2J2. Similarly, MBI was established for amiodarone and NDEA with respect to CYP3A4 but not CYP2J2. On the basis of our reported K_i values (Table 2), both amiodarone and NDEA exhibited similar potencies for mixed competitive inhibition against CYP3A4, whereas dronedarone was a relatively more potent inhibitor of both CYP3A4 and CYP2J2 as compared with NDBD. For MBI, our results confirmed that the inactivation efficiency of NDEA was approximately 3-fold higher than that of amiodarone against CYP3A4 (Table 3). Between dronedarone and NDBD, dronedarone exhibited a stronger inactivation efficiency against CYP3A4 compared with NDBD, whereas both dronedarone and NDBD demonstrated comparable CYP2J2 inactivation efficiency (Table 3).

Using two concentrations of rivaroxaban as the test substrate, our monolayer efflux studies also illustrated the noncompetitive allosteric inhibition of P-gp–mediated rivaroxaban efflux by amiodarone. This finding corroborated previous in silico studies, which also predicted amiodarone to inhibit P-gp by noncompetitive allosteric inhibition (Seelig and Landwojtowicz, 2000). Based on the structural similarities of NDEA to amiodarone, NDEA was assumed to follow a similar mode of P-gp inhibition. Intriguingly, although dronedarone was determined to be a competitive inhibitor of P-gp efflux, NDBD demonstrated a

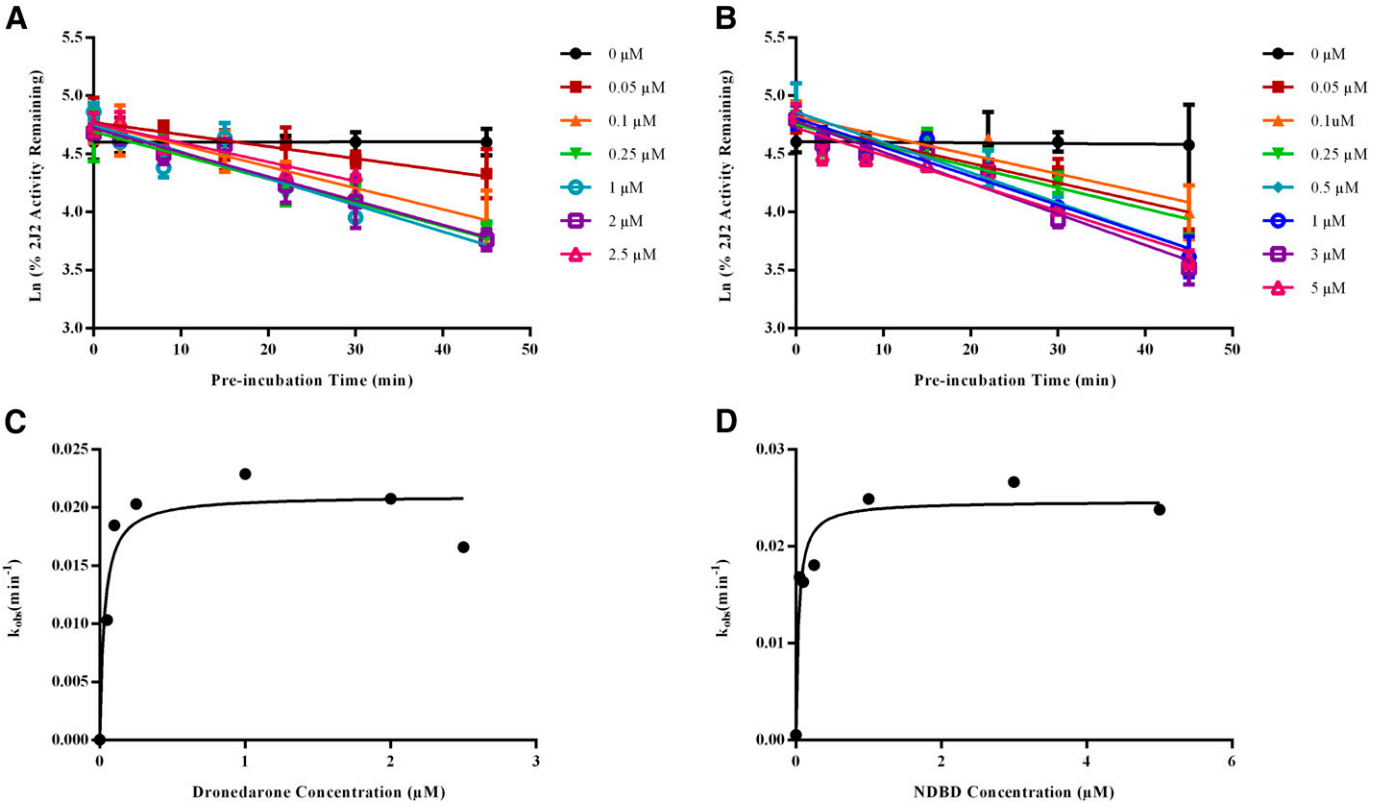

Fig. 4. (A and B) Time- and concentration-dependent inactivation of recombinant CYP2J2 by (A) dronedarone and (B) NDBD using rivaroxaban as the probe substrate. (C and D) Observed inactivation rates (k_{obs}) were plotted against inactivator concentrations to calculate the inactivation kinetic constants, k_{inact} and K_I, for (C) dronedarone and (D) NDBD, respectively. Each point in (A) and (B) represents the mean ± S.D. of triplicate experiments.

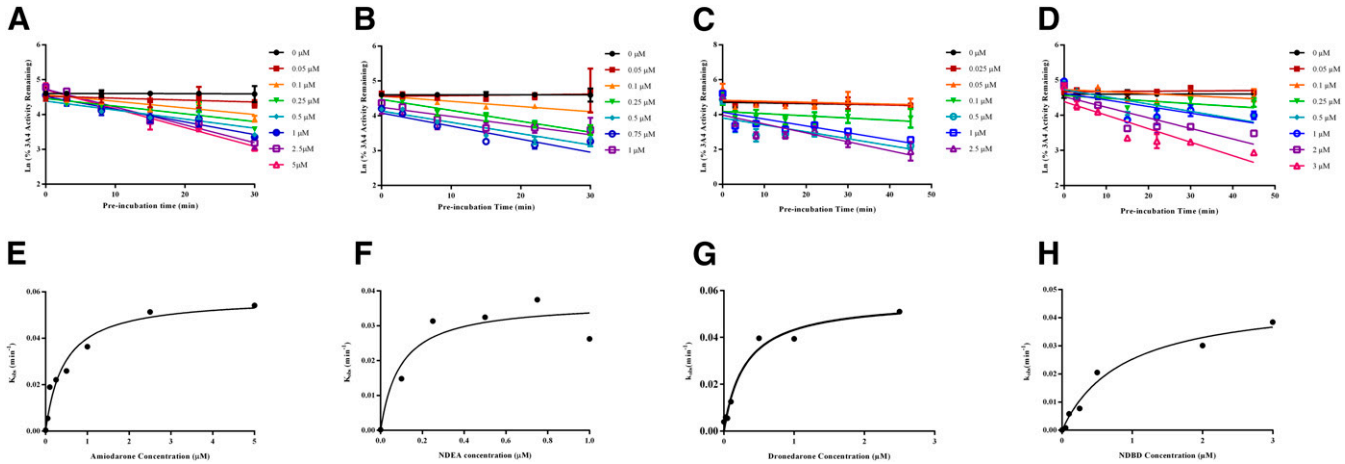

Fig. 5. (A–D) Time- and concentration-dependent inactivation of recombinant CYP3A4 by (A) amiodarone, (B) NDEA, (C) dronedarone, and (D) NDBD using rivaroxaban as the probe substrate. (E–H) Observed inactivation rates (k_{obs}) were plotted against inactivator concentrations to calculate the inactivation kinetic constants, k_{inact} and K_I, for (E) amiodarone, (F) NDEA, (G) dronedarone, and (H) NDBD, respectively. Each point in (A) to (D) represents the mean ± S.D. of triplicate experiments.

minimal inhibitory effect on P-gp (IC_{50} = 76.3 μM). This observation deviates from previous postulation that dronedarone and NDBD may have a potential additive to synergistic effect on P-gp inhibition as is the case with amiodarone and NDEA (FDA, 2009b).

The systemic exposures of NDEA and NDBD are comparable to that of their parent compounds, and regulatory guidance proposes that metabolites present at ≥ 25% of the AUC of the parent drug warrant further consideration with regard to their potential in precipitating in vivo DDIs (FDA, 2012). Taken together, our results indeed underscore the potential contributions of NDEA and NDBA as inhibitory metabolites. NDEA (k_{inact}/K_I = 387 min^{-1}/mM^{-1}) being a more potent time-dependent inactivator of CYP3A4 compared with amiodarone (k_{inact}/K_I = 130 min^{-1}/mM^{-1}) was consistent with previous in vitro studies using midazolam as a probe substrate (McDonald et al., 2015). Likewise, NDEA (K_i = 5.36 μM) being more potent than amiodarone (K_i = 8.94 μM) in the inhibition of P-gp–mediated rivaroxaban transport was also well aligned with previous transport assays using digoxin as a probe substrate (Katoh et al., 2001). In summary, it is evident that a holistic prediction of in vivo clinical DDIs would require consideration of the combined inhibitory effects of both the parent compound and its metabolite.

Comparison of inactivation parameters obtained in our study with previous in-house data generated using FDA-validated probe substrates established a probe substrate differential response (Supplemental Table 3). In the case of CYP3A4, the inactivation efficiency (k_{inact}/K_I) of dronedarone and NDBD was greater when rivaroxaban was used as the probe substrate (i.e., 185 and 53.7 min^{-1}/mM^{-1}) as compared with testosterone (i.e., 44.8 and 15.9 min^{-1}/mM^{-1}). This phenomenon of probe substrate-dependent inhibition profiles has been emphasized mainly for CYP3A4, which possesses multiple probe substrate binding regions within its active site (Kenworthy et al., 1999). Consequently, the interactions observed with one CYP3A4 probe may not accurately reflect those observed with another probe substrate (Galetin et al., 2005; Foti et al., 2010). Although CYP2J2 metabolism is generally restricted to a single active site, our findings suggested differential binding and metabolism among different substrates. Previous studies utilizing FDA-recommended astemizole demonstrated both reversible and irreversible inhibition of CYP2J2 metabolism by amiodarone (Lee et al., 2012). However, our investigation revealed that amiodarone did not inhibit CYP2J2 reversibly and irreversibly with rivaroxaban as the probe substrate (Supplemental Figs. 3, A and B), suggesting the possibility of independent access of the active site of CYP2J2 by amiodarone and rivaroxaban (Shou et al., 1994).

Taken together, our study 1) reiterates that the variability of in vitro inhibitory potencies against CYP3A4 and CYP2J2 is highly dependent on the choice of probe substrates and 2) confirms the importance of using a specific victim drug as the probe substrate in enzyme and transporter interaction studies.

In our study, the static prediction of DDIs between amiodarone, dronedarone, and rivaroxaban yielded an AUC fold change of 1.22 and 1.17, respectively when inhibition of hepatic metabolism was considered (Table 4). On the basis of FDA (2012) guidelines (Table 5), this would imply that no significant inhibition was present. However, upon inclusion of gut metabolism, amiodarone and dronedarone were predicted to precipitate an AUC fold change in rivaroxaban exposure by 1.37 and 1.31, respectively. This attests to the significance of intestinal wall metabolism (Galetin et al., 2007), which when ignored can underestimate the extent of DDIs involving CYP3A4. In addition, our results underscore the potential contribution of NDEA and NDBD to the eventual DDI magnitude, where AUC fold changes of 1.22 and 1.26 were observed, respectively. Furthermore, the inhibition of P-gp– mediated rivaroxaban efflux by amiodarone, NDEA, and dronedarone was also predicted to independently produce AUCR increases of 1.09, 1.13, and 1.09, respectively. However, the simultaneous influences of both parent drug and metabolite as well as the cumulative impact of enzyme-transporter interplay cannot be incorporated in the current static modeling. Moreover, there is also no consensus

TABLE 3

CYP3A4 and CYP2J2 inactivation kinetic parameters for amiodarone, NDEA, dronedarone, and NDBD using morpholinone hydroxylation of rivaroxaban as a surrogate measurement of residual enzymatic activity

Data represent means ± S.D.

P450	K_I	k_{inact}	k_{inact}/K_I
	μM	min^{-1}	min^{-1}/mM^{-1}
CYP3A4			
Amiodarone	0.45 ± 0.12	0.058 ± 0.0045	129
NDEA	0.095 ± 0.070	0.037 ± 0.0056	389
Dronedarone	0.30 ± 0.087	0.056 ± 0.0046	185
NDBD	0.88 ± 0.26	0.047 ± 0.0052	53.7
CYP2J2			
Amiodarone	NA	NA	NA
NDEA	NA	NA	NA
Dronedarone	0.031 ± 0.017	0.021 ± 0.0017	677
NDBD	0.037 ± 0.014	0.025 ± 0.0014	676

NA, not applicable.

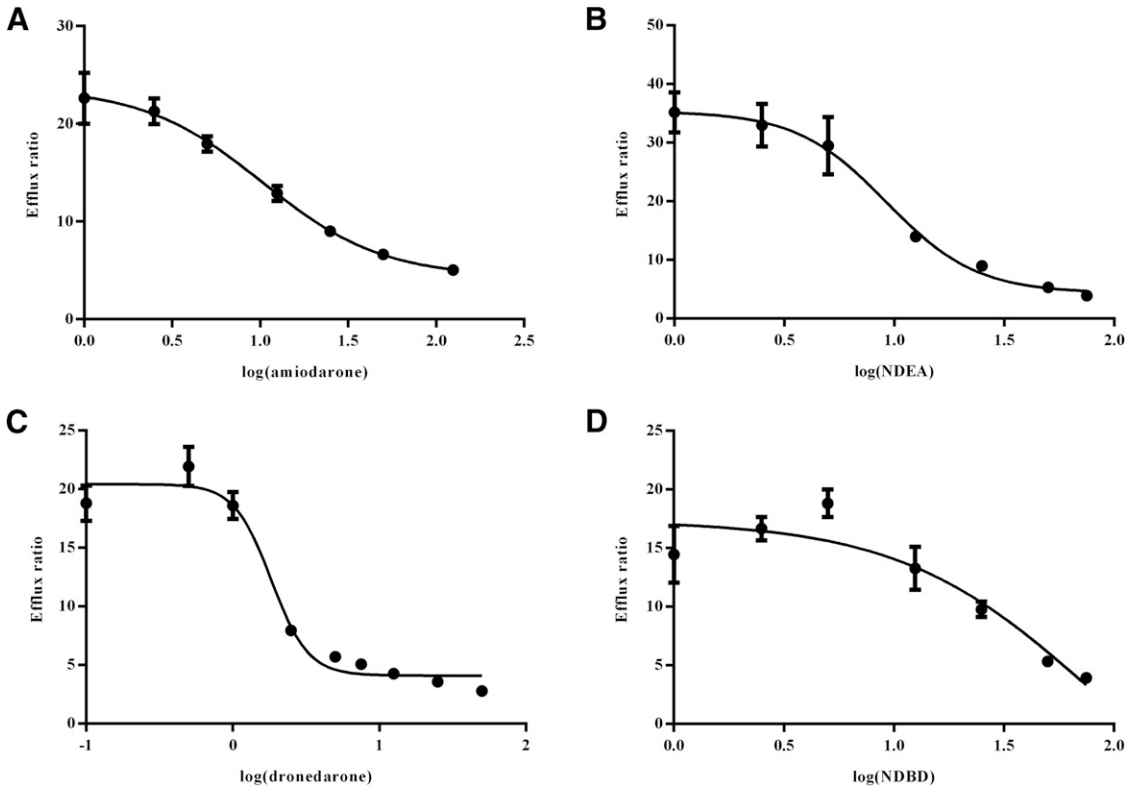

Fig. 6. Inhibition of P-gp–mediated transport of 10 μM rivaroxaban by amiodarone, NDEA, dronedarone, and NDBD. IC_{50} values, determined by nonlinear regression, are (A) 10.3 μM for amiodarone, (B) 9.20 μM for NDEA, (C) 1.83 μM for dronedarone, and (D) 76.3 μM for NDBD. Each point represents the mean ± S.D. of triplicate experiments.

on an appropriate surrogate concentration of the inactivator/inhibitor $[I]_{\text{in vivo}}$ available to the enzyme. Typically, measures of $[I]_{\text{in vivo}}$ are selected based on the estimates that provide the best correlation between predicted and observed DDIs reported in literature (Fahmi et al., 2008). Yet, in our case, our model cannot be cross-validated, since clinical interaction data between rivaroxaban and amiodarone or dronedarone are not available. Nevertheless, it has been shown that model predictability was optimal when free portal steady-state $C_{\max}$ was used for the reversible inhibition portion of the expression (term B) and free systemic steady-state $C_{\max}$ was used for the time-dependent inactivation portion (term A) (Fahmi et al., 2009). Hence, these validated estimates of $[I]_{\text{in vivo}}$ were adopted in our study to enhance DDI predictability.

Given that the in vivo interactions might culminate in a more significant DDI than that estimated using mechanistic static modeling, the use of PBPK models presents several theoretical advantages. First, PBPK modeling utilizes a dynamic approach that allows consideration of changes in concentrations of enzyme, substrate, and inactivator/inhibitor with time, instead of relying on static point estimates. Second, PBPK modeling allows the evaluation of both intrinsic (e.g., organ dysfunction, age, genetics) and extrinsic (e.g., DDIs) factors, alone or in combination, on drug exposure. Third, DDIs across multiple pathways and the variability of these DDIs in different populations can be examined.

Another factor that could potentially affect the in vitro to in vivo correlation is the presence of nonspecific protein binding. The K_i, K_I, and k_{inact} values were computed without accounting for protein binding in the recombinant system. However, Ishigam et al. (2001) reported how the conversion of inhibition constants to their unbound values could eventually lead to more accurate predictions of the AUC fold change upon coadministration of drugs. Furthermore, considering the high protein binding of amiodarone, dronedarone, and their metabolites, the derived in vitro inhibition and inactivation parameters might be relatively higher when unbound concentrations are considered. Hence, to increase confidence in the DDI prediction, the fraction unbound in each incubation should be determined either computationally (Austin et al., 2002) or through equilibrium dialysis experiments (Banker et al., 2003).

TABLE 4

Prediction of metabolic and transporter-mediated DDI upon concomitant administration of rivaroxaban with amiodarone, dronedarone, and their metabolites using mechanistic static modeling

Precipitant	Predicted AUC Fold Change		
	Inhibition of Hepatic Metabolism	Inhibition of Hepatic and Gut Metabolism	Inhibition of P-gp–Mediated Efflux
Amiodarone	1.22	1.37	1.09
NDEA	1.22	NA	1.13
Dronedarone	1.17	1.31	1.09
NDBD	1.26	NA	ND

NA, not applicable; ND, not determined.

TABLE 5

FDA guidelines for relative risk of DDIs based on observed increases in AUC for the victim drug

Category of Relative Risk	Observed Changes in AUC
Strong DDI	≥5-fold increase in AUC
Moderate DDI	≥2 but <5-fold increase in AUC
Weak DDI	≥1.25 but <2-fold increase in AUC

In conclusion, amiodarone, dronedarone, NDEA, and NDBD cause reversible inhibition and irreversible MBI of CYP3A4 with rivaroxaban as the probe substrate. Amiodarone and NDEA, unlike dronedarone and NDBD, do not inhibit CYP2J2. Amiodarone, dronedarone, and NDEA, but not NDBD, inhibit P-gp–mediated efflux of rivaroxaban. Static modeling predicted a weak DDI risk between rivaroxaban and amiodarone or dronedarone. Fundamental limitations of the static model implied that molecular interactions between rivaroxaban and the antiarrhythmic agents and their metabolites via CYP3A4, CYP2J2, and P-gp were not considered in entirety. Future work would involve the assimilation of these in vitro inhibition parameters into a dynamic PBPK model, from which a more accurate quantitation of DDI magnitude can be derived.

Authorship Contributions

Participated in research design: Cheong, Goh, Hong, Kojodjojo, Chan.

Conducted experiments: Cheong, Goh, Hong, Venkatesan, Liu.

Contributed new reagents or analytic tools: Chiu.

Performed data analysis: Cheong, Goh, Hong, Chan.

Wrote or contributed to the writing of the manuscript: Cheong, Goh, Hong, Chan.

References

Austin RP, Barton P, Cockroft SL, Wenlock MC, and Riley RJ (2002) The influence of nonspecific microsomal binding on apparent intrinsic clearance, and its prediction from physicochemical properties. *Drug Metab Dispos* **30**:1497–1503.

Banker MJ, Clark TH, and Williams JA (2003) Development and validation of a 96-well equilibrium dialysis apparatus for measuring plasma protein binding. *J Pharm Sci* **92**:967–974.

Chugh SS, Havmoeller R, Narayanan K, Singh D, Rienstra M, Benjamin EJ, Gillum RF, Kim YH, McAnulty JH, Jr, Zheng ZJ, et al. (2014) Worldwide epidemiology of atrial fibrillation: a Global Burden of Disease 2010 Study. *Circulation* **129**:837–847.

Fabre G, Julian B, Saint-Aubert B, Joyeux H, and Berger Y (1993) Evidence for CYP3A-mediated N-deethylation of amiodarone in human liver microsomal fractions. *Drug Metab Dispos* **21**: 978–985.

Fahmi OA, Hurst S, Plowchalk D, Cook J, Guo F, Youdim K, Dickins M, Phipps A, Darekar A, Hyland R, et al. (2009) Comparison of different algorithms for predicting clinical drug-drug interactions, based on the use of CYP3A4 in vitro data: predictions of compounds as precipitants of interaction. *Drug Metab Dispos* **37**:1658–1666.

Fahmi OA, Maurer TS, Kish M, Cardenas E, Boldt S, and Nettleton D (2008) A combined model for predicting CYP3A4 clinical net drug-drug interaction based on CYP3A4 inhibition, inactivation, and induction determined in vitro. *Drug Metab Dispos* **36**: 1698–1708.

FDA (2009a) *Multaq (Dronedarone) Briefing Document*, U.S. Food and Drug Administration, Silver Spring, MD.

FDA (2009b) *Multaq (Dronedarone) Clinical Pharmacology and Biopharmaceutics Review*, U.S. Food and Drug Administration, Silver Spring, MD.

FDA (2011a) *Xarelto (Rivaroxaban) Clinical Pharmacology and Biopharmaceutics Review*, U.S. Food and Drug Administration, Silver Spring, MD.

FDA (2011b) *Xarelto (Rivaroxaban) Product Information*, U.S. Food and Drug Administration, Silver Spring, MD.

FDA (2012) *Guidance for Industry, Drug Interaction Studies—Study Design, Data Analysis, Implications for Dosing, and Labeling Recommendations*, U.S. Food and Drug Administration, Silver Spring, MD.

Feng B, Hurst S, Lu Y, Varma MV, Rotter CJ, El-Kattan A, Lockwood P, and Corrigan B (2013) Quantitative prediction of renal transporter-mediated clinical drug-drug interactions. *Mol Pharm* **10**:4207–4215.

Foti RS, Rock DA, Wienkers LC, and Wahlstrom JL (2010) Selection of alternative CYP3A4 probe substrates for clinical drug interaction studies using in vitro data and in vivo simulation. *Drug Metab Dispos* **38**:981–987.

Galetin A, Hinton LK, Burt H, Obach RS, and Houston JB (2007) Maximal inhibition of intestinal first-pass metabolism as a pragmatic indicator of intestinal contribution to the drug-drug interactions for CYP3A4 cleared drugs. *Curr Drug Metab* **8**:685–693.

Galetin A, Ito K, Hallifax D, and Houston JB (2005) CYP3A4 substrate selection and substitution in the prediction of potential drug-drug interactions. *J Pharmacol Exp Ther* **314**:180–90.

Gnoth MJ, Buetehorn U, Muenster U, Schwarz T, and Sandmann S (2011) In vitro and in vivo P-glycoprotein transport characteristics of rivaroxaban. *J Pharmacol Exp Ther* **338**:372–380.

Grillo JA, Zhao P, Bullock J, Booth BP, Lu M, Robie-Suh K, Berglund EG, Pang KS, Rahman A, Zhang L, et al. (2012) Utility of a physiologically-based pharmacokinetic (PBPK) modeling approach to quantitatively predict a complex drug-drug-disease interaction scenario for rivaroxaban during the drug review process: implications for clinical practice. *Biopharm Drug Dispos* **33**:99–110.

Hong Y, Chia YMF, Yeo RH, Venkatesan G, Koh SK, Chai CLL, Zhou L, Kojodjojo P, and Chan ECY (2016) Inactivation of human cytochrome P450 3A4 and 3A5 by dronedarone and N-desbutyl dronedarone. *Mol Pharmacol* **89**:1–13.

Ishigam M, Uchiyama M, Kondo T, Iwabuchi H, Inoue S, Takasaki W, Ikeda T, Komai T, Ito K, and Sugiyama Y (2001) Inhibition of in vitro metabolism of simvastatin by itraconazole in humans and prediction of in vivo drug-drug interactions. *Pharm Res* **18**:622–631.

Isoherranen N, Lutz JD, Chung SP, Hachad H, Levy RH, and Ragueneau-Majlessi I (2012) Importance of multi-p450 inhibition in drug-drug interactions: evaluation of incidence, inhibition magnitude, and prediction from in vitro data. *Chem Res Toxicol* **25**:2285–2300.

January CT, Wann LS, Alpert JS, Calkins H, Cigarroa JE, Conti JB, Ellinor PT, Ezekowitz MD, Field ME, Murray KT, Sacco RL, et al. (2014) 2014 AHA/ACC/HRS guideline for the management of patients with atrial fibrillation. *J Am Coll Cardiol* **63**:e1–e76.

Karkhanis A, Lam HY, Venkatesan G, Koh SK, Chai CLL, Zhou L, Hong Y, Kojodjojo P, and Chan ECY (2016) Multiple modes of inhibition of human cytochrome P450 2J2 by dronedarone, amiodarone and their active metabolites. *Biochem Pharmacol* **107**:67–80.

Katoh M, Nakajima M, Yamazaki H, and Yokoi T (2001) Inhibitory effects of CYP3A4 substrates and their metabolites on P-glycoprotein-mediated transport. *Eur J Pharm Sci* **12**:505–513.

Kenworthy KE, Bloomer JC, Clarke SE, and Houston JB (1999) CYP3A4 drug interactions: Correlation of 10 in vitro probe substrates. *Br J Clin Pharmacol* **48**:716–727.

Klieber S, Arabeyre-Fabre C, Moliner P, Marti E, Mandray M, Ngo R, Ollier C, Brun P, and Fabre G (2014) Identification of metabolic pathways and enzyme systems involved in the in vitro human hepatic metabolism of dronedarone, a potent new oral antiarrhythmic drug. *Pharmacol Res Perspect* **2**:e00044.

Lee CA, Jones JP, 3rd, Katayama J, Kaspera R, Jiang Y, Freiwald S, Smith E, Walker GS, and Totah RA (2012) Identifying a selective substrate and inhibitor pair for the evaluation of CYP2J2 activity. *Drug Metab Dispos* **40**:943–951.

Lee CA, Neul D, Clouser-Roche A, Dalvie D, Wester MR, Jiang Y, Jones JP, 3rd, Freiwald S, Zientek M, and Totah RA (2010) Identification of novel substrates for human cytochrome P450 2J2. *Drug Metab Dispos* **38**:347–356.

McDonald MG, Au NT, and Rettie AE (2015) P450-based drug-drug interactions of amiodarone and its metabolites: diversity of inhibitory mechanisms. *Drug Metab Dispos* **43**:1661–1669.

Mueck W, Stampfuss J, Kubitza D, and Becka M (2014) Clinical pharmacokinetic and pharmacodynamic profile of rivaroxaban. *Clin Pharmacokinet* **53**:1–16.

Ohyama K, Nakajima M, Suzuki M, Shimada N, Yamazaki H, and Yokoi T (2000) Inhibitory effects of amiodarone and its N-deethylated metabolite on human cytochrome P450 activities: prediction of in vivo drug interactions. *Br J Clin Pharmacol* **49**:244–253.

Orr STM, Ripp SL, Ballard TE, Henderson JL, Scott DO, Obach RS, Sun H, and Kalgutkar AS (2012) Mechanism-based inactivation (MBI) of cytochrome P450 enzymes: structure-activity relationships and discovery strategies to mitigate drug-drug interaction risks. *J Med Chem* **55**:4896–4933.

Rahman F, Kwan GF, and Benjamin EJ (2014) Global epidemiology of atrial fibrillation. *Nat Rev Cardiol* **11**:639–654.

Seelig A and Landwojtowicz E (2000) Structure-activity relationship of P-glycoprotein substrates and modifiers. *Eur J Pharm Sci* **12**:31–40.

Shou M, Grogan J, Mancewicz JA, Krausz KW, Gonzalez FJ, Gelboin HV, and Korzekwa KR (1994) Activation of CYP3A4: evidence for the simultaneous binding of two substrates in a cytochrome P450 active site. *Biochemistry* **33**:6450–6455.

Steinberg BA, Hellkamp AS, Lokhnygina Y, Halperin JL, Breithardt G, Passman R, Hankey GJ, Patel MR, Becker RC, Singer DE, et al.; ROCKET AF Steering Committee and Investigators (2014) Use and outcomes of antiarrhythmic therapy in patients with atrial fibrillation receiving oral anticoagulation: results from the ROCKET AF trial. *Heart Rhythm* **11**:925–932.

Weinz C, Schwarz T, Kubitza D, Mueck W, and Lang D (2009) Metabolism and excretion of rivaroxaban, an oral, direct factor Xa inhibitor, in rats, dogs, and humans. *Drug Metab Dispos* **37**:1056–1064.

Yang J, Liao M, Shou M, Jamei M, Yeo KR, Tucker GT, and Rostami-Hodjegan A (2008) Cytochrome P450 turnover: regulation of synthesis and degradation, methods for determining rates, and implications for the prediction of drug interactions. *Curr Drug Metab* **9**:384–394.

Zhang L, Zhang YD, Zhao P, and Huang S-M (2009) Predicting drug-drug interactions: an FDA perspective. *AAPS J* **11**:300–306.

Address correspondence to: Eric Chun Yong Chan, Department of Pharmacy, Faculty of Science, National University of Singapore, Block S7, Level 2, 18 Science Drive 4, Singapore 117543, Singapore. E-mail: phaccye@nus.edu.sg